International Journal of Scientific Research in Engineering and Management (IJSREM)
Volume: 03 Issue: 09 | Sept -2019 ISSN: 2590-1892

High-efficiency micro robotic fly

Vishnu Prasad A R

I. INTRODUCTION

Regarding nature's smallest fliers, contemporary studies have given detailed insights into the remarkable maneuverability of some flying insects. Insects encompass the most agile flying objects on earth, including all things man-made and biological. Until recently, the aerodynamic mechanisms by which insects achieve this performance were not understood in the framework of classical aerodynamic theory. The complex aerodynamics of a periodic wing stroke at low Reynolds numbers (less than 1000) is understood well enough to be used as a design tool for engineers that wish to recreate these devices.

But, this understanding is not sufficient to create effective robotic insects. Novel manufacturing paradigms must be considered concurrently in order to achieve the level of efficiency and durability that millimeter-scale flying machines will require. The high speed, highly articulated mechanisms that are necessary to reproduce insect-like wing motions exist on a scale that is between micro-electromechanical systems (MEMS) and "macro" devices. Thus, a "meso" scale rapid fabrication method, called smart composite microstructures (SCMs), is used to bridge this gap. Previous research has yielded concise design rules for the development of flexure-based micromechanical structures based upon the SCM process. These design rules form the basis for the device that is described here: an insect-sized flapping-wing micro air vehicle (MAV).

Insect-like vehicles have vast potential applications including search and rescue, hazardous environment exploration, surveillance, reconnaissance, and planetary exploration.

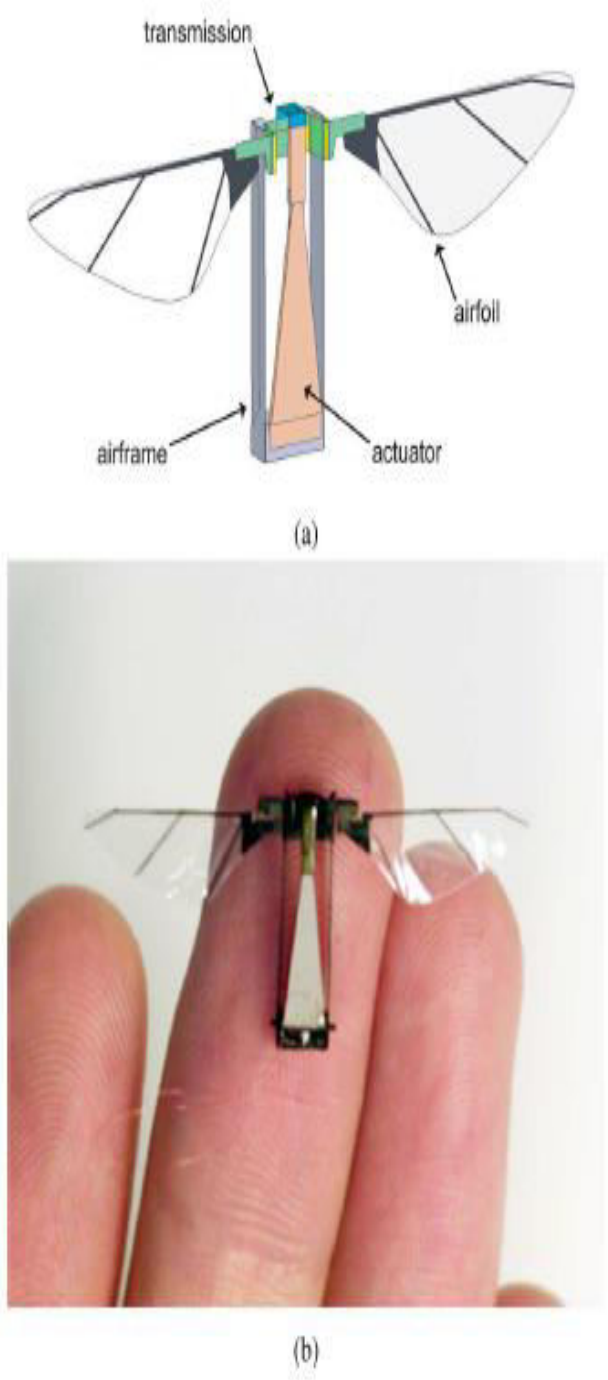

Fig.1.(a) Conceptual drawing highlighting the four primary mechanical and aeromechanical components. (b) First insect-scale flying robot able to takeoff.

II. INSECT FLIGHT

Insects of the order Diptera generate aerodynamic forces with a three degree-of-freedom wing trajectory that consists of a large wing stroke (that defines the stroke plane), pronation and supination (collectively called wing rotation) about a longitudinal wing axis, and stroke plane deviation . This discussion will not consider stroke plane deviation: for some hovering Dipteran insects that have a nearly horizontal stroke plane, it does not appear that stroke plane deviation plays a significant role in lift generation. This considerably simplifies the analysis of the wing trajectory and the construction of the transmission mechanism. The desired two degree-of-freedom trajectory profile is shown in Fig. 2(a). Dipteran insects generate wing motions using indirect flight muscles that pull on a deformable section of the exoskeleton called the scutum . The wing is connected to the pleural wing process at the interface of the scutum and the exoskeleton. Contractions of the dorso-ventral muscles depress the scutum and create the upstroke. Contractions of the dorso-longitudinal muscles shorten the thorax and return the scutum to its initial position, generating the down stroke [see Fig. 2(b) and (c)]. Wing rotation is accomplished by smaller muscles (basalar and subalar) that directly apply a torque to the sclerites connected to the wing hinge. While there has been some debate over the concise

mechanisms involved in Dipteran thoracicmechanics, there are a few clear characteristics of the wing drive system.

1) Insects utilize aero-mechanical advantage to amplify the wing stroke.

2) Diptera operates their wing strokes at the natural frequency of the aeromechanical system.

3) Some aspects of Dipteran wing trajectories are mechanically "hard-coded" into their morphologies while others are tunable.

Here, we utilize each of these aspects with the creation of a resonant wing-drive system that is mechanically "preprogrammed" with a desired baseline trajectory. A parallel is shown in Fig. 2(b)–(e) between Dipteran thoracic morphology (oversimplified) and the robotic version.

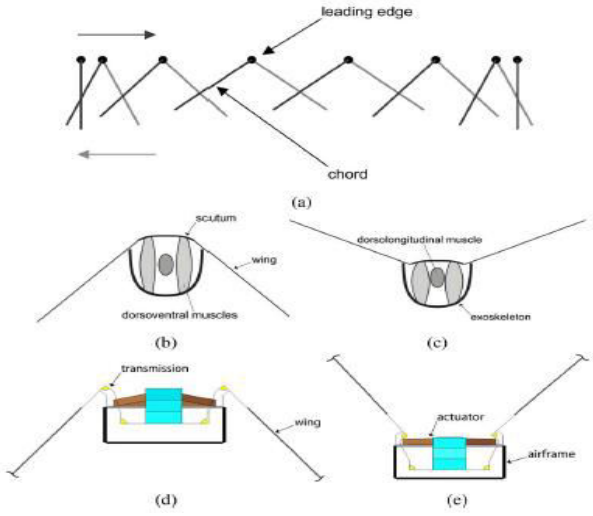

Fig. 2. Approximate wing motion: (a) projected onto a 2-D plane (ignoring stroke plane deviation) along with a diagram of a Dipteran insect thorax showing generation of down stroke (b) and upstroke (c). For comparison, the anterior diagram of the robotic thorax motion is also shown. The wing moves from the lower extreme (d) to the upper (e) by linear actuator motions coupled through a flexure-based transmission.

III. CREATION OF A ROBOTIC INSECT

Insect wing trajectories are the basis for the Harvard Micro-robotic Fly. If a robotic device can reproduce the necessary aspects of Dipteran wing motion with a similar wing-beat frequency and mass comparable to actual flies, it should be capable of producing sufficient thrust to fly. This device has four primary mechanical components: the airframe (exoskeleton), actuator (flight muscle), transmission (thorax), and airfoils, as is shown in Fig. 1(a). The functions of each are simple:

1) The airframe provides a solid ground to the actuator and transmission while contributing minimal mass;

2) The actuator should provide motion with maximal power density;

3) The transmission must efficiently impedance-match the actuator to the load; and

4) The airfoils must remain rigid to hold shape under large aerodynamic loads. The

subtleties of these components are described later.

A. Actuation

There is one primary actuator that drives the thorax in a similar configuration to Dipteran dorso-ventral muscles, but with bidirectional force. The actuator chosen for this application is a bimorph piezoelectric clamped-free bending cantilever that is optimized for mechanical power delivery and created using SCM. These actuators are chosen because of favorable scalability (compared, for example, to electromagnetic motors) and compatibility with the SCM process. Compared to other actuation technologies, piezoelectric actuators typically have high operating stresses and frequencies. However, piezo-ceramic materials are dense and brittle and typically achieve relatively small strains (hence the need for mechanical amplification). The ultimate quantity of interest for a hover-capable MAV is the power density (at the frequency of interest). For the sake of a performance metric, biological estimates place the body-mass-specific power density for flying insects between 29 W/kg and 40 W/kg and between 80 W/kg and 83 W/kg for the muscles alone. For comparison, the classes of actuators used here have demonstrated power densities of 400 W/kg. This is the first example of where a subsystem of the micro-robotic fly exceeds the performance of its biological counterpart.

The design of the actuator is based upon a laminate plate theory model that describes the stress distribution across a multilayered composite structure (see for details of this model). Since the individual layers are thin, the model is simplified to a reduced-tensor notation. However, all desired characteristics of the actuator are included (e.g., displacement, peak force, bandwidth, etc.). The actuators are created with the SCM process: first, individual lamina [PbZrTiO3 (PZT)-5H and M60J carbon fiber/cyanate ester resin prepreg] are laser-micromachined into desired planform shapes. These layers [see Fig. 3(a)] are then stacked and aligned and put through a controlled cure cycle that regulates temperature, pressure, and time of cure. The resulting actuator is fixed to the airframe proximally and the input to the transmission distally. Application of an electric field creates a bending moment in the actuator that deflects the transmission [exaggerated in Fig. 3(b)]. These actuators are 40 mg, 12 mm long, and achieve a deflection of greater than ±400 μm with a bandwidth greater than 1 kHz.

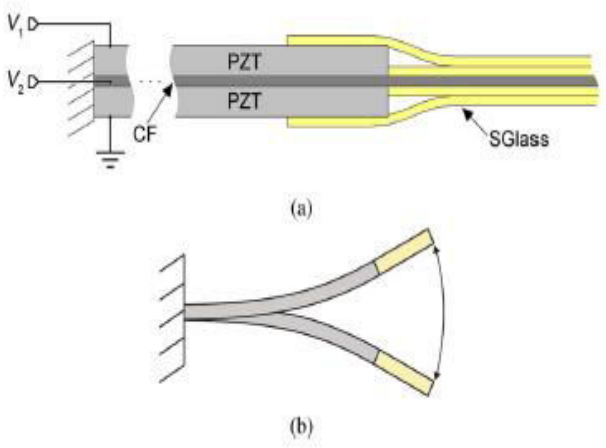

Fig. 3. Overview of the flight muscles used for the Harvard Micro-robotic fly. (a) Clamped-free bending cantilever that consists of symmetric layers of laser-micromachined piezo-ceramic PbZrTiO3 (PZT). (b) Actuator bends (shown exaggerated) as an electric field is applied to either plate.

B. Transmission

Similar to the insect model shown in Fig. 2(b) and (c), the transmission amplifies the actuator motion from a translational input to a rotational output. This is done while impedance matching the load to the actuator: the system is driven at its fundamental resonance, and thus, the dynamics during normal operation are dominated by the wing loading and the actuator losses. Therefore, for efficient electromechanical transduction, it is imperative that the wing loading (as seen by the actuator) is matched to the internal losses of the actuator.

At larger scales, such a device could be assembled with gears and slider mechanisms. However, due to unfavorable surface area scaling, such components would result in significant friction losses as the characteristic size is decreased. Instead, flexures are used in place of revolute joints (see Fig. 4). The desired stroke amplitude is ±60◦; thus, for actuator motion of approximately ±400 μm, we require a transmission that has a nominal amplification of approximately 2600 rad/m. This is called the *transmission ratio* and is directly analogous to a gear ratio for these compliant mechanisms. Note that this assumes a perfectly compliant transmission. If the stiffness of the transmission is nonzero, the transmission ratio will need to be increased.

There has been significant research into the creation and characterization of flexure-based micromechanical devices, and these design rules provide the basis for the creation of the transmission. These flexure mechanisms are also created using the SCM paradigm. To create jointed structures, rigid materials (carbon fiber reinforced composite prepregs) are cut as face sheets and polymers (typically polyimide) are used as the flexure. These are again bonded in a controlled cure cycle. This mechanism is shown in Figs. 2(d) and (e) and 5(a).

The actuator and transmission directly control the wing stroke. Wing rotation is developed passively with an additional flexure positioned between the output of the transmission

and thewing. This flexure is parallel to the spanwise direction and includes joint-stops to avoid over-rotation [see Fig. 5(c)]. Thus, this system has three degrees-of-freedom, only one of which is actuated (as opposed to concurrent research on insect-inspired MAVs that attempt to concisely control each degree-of-freedom independently).

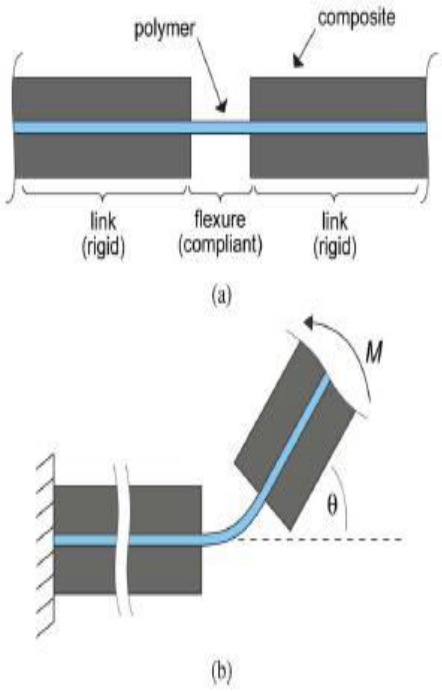

Fig. 4. Cross section of a typical flexure joint used in the thorax of the Harvard Microrobotic Fly. (a) Laser-micromachined carbon fiber reinforced composite face sheets sandwich a thin layer of polyimide. (b) Compliance of the joint is determined by the geometry and material properties such that a moment, M, results in an angular deflection, θ.

C. Airfoils

The airfoils are designed to match the shape and size of the wings of Syrphid hoverflies. Insect wings have nontrivial anisotropic compliances, but the airfoils used here are designed to remain rigid for all expected loading conditions. The airfoils are morphologically similar to insect wings; however, the "veins" consist of 30 μm thick ultrahigh modulus carbon fiber reinforced composite beams and the membrane" is 1.5 μm thick polyester. The veins are arranged so that the wing is extremely rigid over the expected range of flight forces. To enable quasi-static passive wing rotation, the rotational inertia must be low such that the rotational resonant frequency is sufficiently high. Assuming under-damped second-order dynamics, an acceptable criterion for quasi-static rotation is that the first 3 dB point for rotation occurs above the flapping frequency. The 15 mm wing shown in Fig. 5(b) weighs 400 μg and remains undeformed during the entire stroke [see Fig. 7(a)]. These wings exhibit a remarkably high stiffness-to-weight ratio, which is a second example of the superiority of a micromechanical device over a biological system (due to significant differences between the material properties of chitin and carbon fiber).

IV. RESULTS

Each of the components of the fly are assembled onto the airframe resulting in the structure shown in various hover-capable species in Fig. 6. The mass of each component in the integrated structure is given in Table I.

component	mass (mg)
actuator	40
transmission	4
wings (×2)	≈0.5
airframe	11
misc. wiring, epoxy, etc.	5
total body	**60**

TABLE II
INTEGRATED MAV PERFORMANCE

total mass	60mg
wingspan	3cm
actuator PD	$>150 \mathrm{Wkg}^{-1}$
total PD	$>100 \mathrm{Wkg}^{-1}$
wing stroke	$> \pm 50^{\circ}$
wing rotation	$\pm 50^{\circ}$
wingbeat frequency	110Hz
peak wing velocity	$> 6 \mathrm{ms}^{-1}$
peak Re	≈1200

Table I: Mass Properties For Each Component Of The Mav

To isolate thrust from roll, pitch, and yaw moments, the robotic fly is fixed to taut guide wires that restrict the fly to purely vertical motion (guides are fabricated into the airframe). These wires are "training wheels" that will be incrementally removed in future research as attitude sensing and control are migrated onboard. The wings are driven open loop at the flapping resonance to maximize the stroke amplitude. For the MAV shown in Fig.1(b). To give an overall perspective, the finished robotic fly is compared to shown in Fig. 1, the resonant frequency is 110 Hz. So long as the rotational frequency is sufficiently higher than the flapping resonant frequency, the rotational component will operate quasi-statically. The natural frequency for wing rotation is calculated to be approximately 250 Hz based upon the flexural stiffness of the wing hinge and the rotational inertia of the wing [estimated from a computer-aided design (CAD) model]. Thus, the aerodynamic and inertial loads act to decrease the angle of attack, and the joint stops assure that the wings do not over-rotate. To visualize the wing motion, a high-speed video camera was used in two perspectives (lateral and anterior). Sequential frames from these videos are shown in Fig. 7. From the original high-speed video (≈20 frames/period), the wing kinematics are extracted (using custom Matlab software) and shown in Fig. 8. The trajectory is nearly identical to that of hovering Dipteran insects that lends credence to the use of passive rotation. However, the primary performance metric is the lift that is generated. This is assessed in two ways. First, the fly is fixed to a custom force sensor and the wings are driven open loop (maximum actuator drive field of 2 Vμm-1). Lift measurement trials start by:

1) Collecting the zero level of the sensor;
2) Starting the wing from rest and allowing transients to decay; and

3) Collecting the force data

Over ten trials, an average lift of 1.14 ±0.23mN is measured, corresponding to a thrust-to-weight ratio of approximately 2. Second, the integrated fly is aligned to the guide wires and allowed to freely move in the vertical direction. The wings are driven open loop and the fly ascends, as is shown in Fig. 9. This marks the first (tethered) liftoff of an insect scale micro-robot and validates the use of biological inspiration.

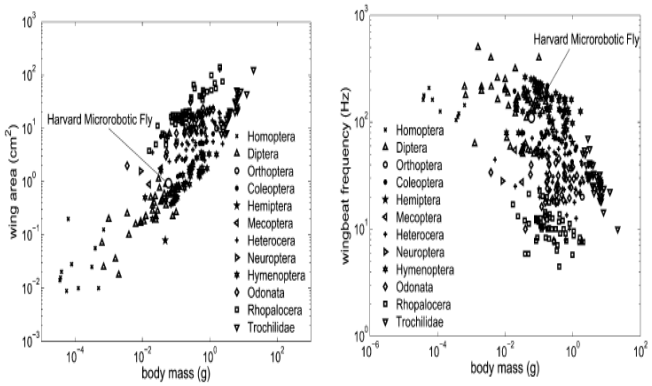

Fig. 6. Morphological and dynamic parameters of hover-capable biological examples as a function of body mass. It is clear that the device described here is consistent with biological trends.

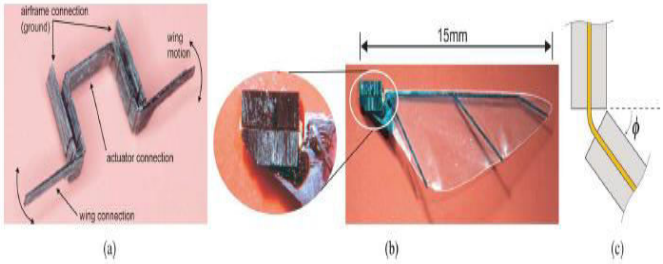

Fig. 6. Morphological and dynamic parameters of hover-capable biological examples as a function of body mass. It is clear that the device described here is consistent with biological trends.

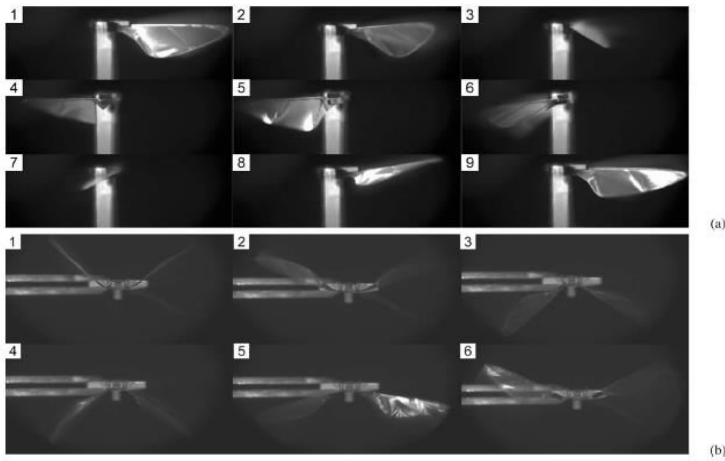

Fig. 7. (a) Wing motion as seen from a lateral perspective. (b) Anterior perspective. Frames are taken from a high-speed video sequence (left to right, top to bottom) of the wing moving at its flapping resonance. The lateral perspective is oriented to the midstroke: note that the symmetry and that the angle of attack at midstroke is approximately 40◦.

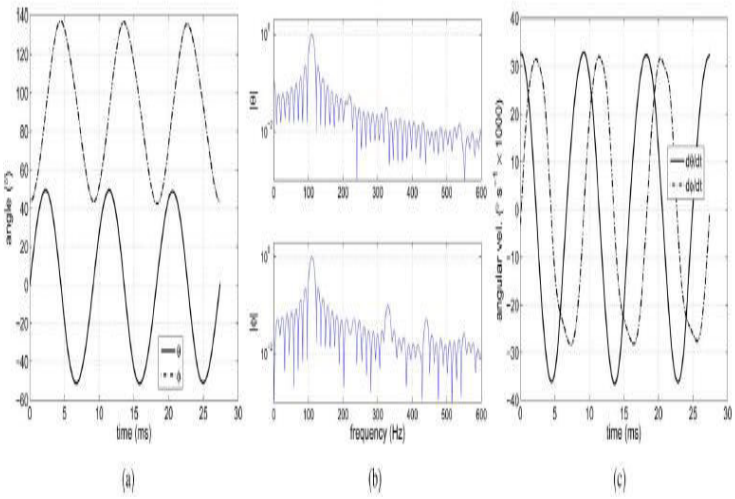

Fig. 8. (a)Wing trajectory extracted from anterior and lateral high-speed video sequences. (b) Flapping (θ) is mostly sinusoidal while rotation (φ) has significant components at other frequencies (most notably the third and fourth harmonics). (c) Angular velocities of the wing [as calculated from the angular positions in (a)].

V. CONCLUSION

In summary, the performance of the Harvard Micro-robotic Fly proves:

1) Generating wing trajectories similar to Dipteran insects is possible with a robotic device and
2) Propulsion generated by this micro-robot is significant (compared to the body mass).

However, these results do not show free flight, integrated sensing and control, or onboard power and electronics. Therefore, the Harvard Micro-robotic Fly only represents a solution to the mechanical and aeromechanical components of an autonomous robotic insect. In order to create a fully autonomous flying micro-robot, there are two additional research challenges that must be solved:

1) High-efficiency sensing, power conditioning, and control microelectronics and
2) A high energy density power source.

In previous work, a suite of biologically inspired sensors appropriate for attitude estimation and control has been developed . This suite consists of sub-10 mg mechano-receptive and hoto-receptive sensors. Future development must evolve these into a monolithic solution for low-level (stabilization) sensors. Power and control electronics must also be created to drive the actuators. Both power and control architectures must be efficient, high bandwidth, and eventually occupy a very small volume of silicon. To compound these requirements, the Piezo-electric actuators used in the Harvard Micro-robotic Fly require high fields (approximately 2 Vμm-1). Efficient, lightweight boost conversion, and drive electronics for these actuators are ongoing research topics.

Fig. 9.First tethered flight of an at-scale robotic insect. From a video sequence spaced at approximately 100 ms intervals.

The final component necessary for a fully autonomous fly is a power source appropriate for both long duration flight and short energetic bursts. Based upon the electrical power requirements for the current fly, estimates of overall efficiency for the final version and the best available battery chemistry, it is estimated that fly-sized robots can operate for 5–10 min. However, this expected flight time is based upon the energy density of large-scale batteries. While there is no reason to expect that the chemistry should change with a decrease in physical dimensions, a decrease in size will result in a larger surface area to volume ratio, and thereby,

require more packaging material for a given volume of battery. Furthermore, these numbers are for hovering in still air conditions. Gusts or air currents will require more power to remain stationary or follow a prescribed trajectory. The flight time will be incrementally increased by improvements in battery technology, increased propulsive efficiency, and the addition of energy harvesting devices (e.g. solar, vibrational, thermal, etc.).

It was noted that the maximum lift-to-weight ratio is approximately 2. However, this is only for the mechanical and aeromechanical structures. To enable the same specific thrust when power, electronics, and control are migrated onboard, we will need to further maximize the propulsive efficiency. For example, doubling the weight of the fly to 120 mg will require twice the current thrust to maintain a thrust-to-weight ratio of 2. This is a current focus that has begun with empirically verified wing modeling and optimization. It is useful at this point to investigate the mass distribution for the fully autonomous fly. This distribution is shown in Fig. 10. Note that in this distribution, the battery represents approximately 40% of the body mass. For Terrestrial mobile robots, greater range can be achieved with a larger, higher capacity power source (within reasonable limits). However, for an aerial robot, this is not true since increased power supply mass will require larger lift forces to sustain flight. This increase in mechanical power translates into a corresponding increase in electrical power, and thus, increasing the battery mass has diminishing returns. The mechanical components in Fig. 10 do not require significant reduction from the current masses given in Table I. With regard to the electrical components, consider that a thinned silicon die with dimensions of 4 mm × 4 mm × 250 μm will have a mass just under 10 mg (with wiring). To put this in perspective, this chip would have twice the area of a 8051 microcontroller and potentially 500 000 transistors. For perspective, a *Drosophila malanogaster* has approximately 300 000 neurons. The development of millimeterscale ultralow energy controllers for autonomous Microsystems has started for sensor network applications.

In earlier sections, there were two allusions to subsystems that outperform biological counterparts. This is by no means universal; there are countless aspects of flying insects that were heretofore unattainable with mechanical recreations. For example, evolution has done a phenomenal job with the integration of actuation, power, and control. However, due in part to recent advances in fabrication techniques (i.e., SCM), this gap is progressively narrowing.

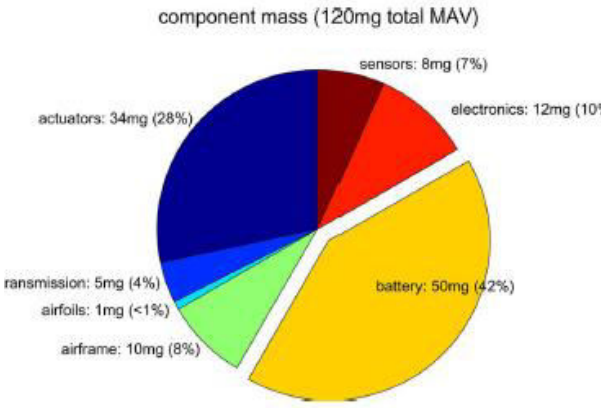

Fig. 10. Distribution of total MAV mass as predicted for the final, fully autonomous insect-scale MAV.

Biological inspiration is ubiquitous in the mechanical subsystems that make up the Harvard Micro-robotic Fly. Because of the relative ease of micro-fabrication allowed by SCM, these micromechanical devices can now be used in the opposite direction to gain insights into biological systems. For example, there are open questions pertaining to the scaling of biological airfoils and their compliances: do performance gains correspond to anisotropic compliances or are airfoil compliances simply due to biological material limitations? This may be a difficult question to answer with biological observation; but, by fabricating micro-robotic airfoils with a large space of physical parameters, we can ascertain the role of compliance in lift generation, propulsive efficiency, stability, etc. This forms a sort of "closed-loop biological inspiration" that could be a valuable tool for biomechanics researchers.

REFERENCES

[1] C. P. Ellington, C. van der Berg, A. P. Willmott, and A. L. R. Thomas, "Leading-edge vortices in insect flight," *Nature*, vol. 384, pp. 626–630, Dec. 1996.

[2] M. H. Dickinson, F.-O. Lehmann, and S. P. Sane, "Wing rotation and the aerodynamic basis of insect flight," *Science*, vol. 284, pp. 1954–1960, Jun. 1999.

[3] R. J. Wood, S. Avadhanula, R. Sahai, E. Steltz, and R. S. Fearing, "Microrobot design using fiber reinforced composites," *J. Mech. Design*, to be published.

[4] J. A. Miyan and A. W. Ewing, "How Diptera move their wings: A reexamination of the wing base articulation and muscle systems concerned with flight," *Phil. Trans. R. Soc. Lond.*, vol. B311, pp. 271–302, 1985.

[5] W. C. Wu, L. Schenato, R. J. Wood, and R. S. Fearing, "Biomimetic sensor suite for flight control of a micromechanical flying insect: Design and experimental results," in *Proc. IEEE Int. Conf. Robot. Autom.*, Taipei, Taiwan, Sep. 2003, vol. 1, pp. 1146–1151.